# High-pressure behavior of Raman modes in $CuGaS_2$

J. González and B. J. Fernández
*Departamento de Física, Centro de Estudios de Semiconductores, Facultad de Ciencias, Universidad de Los Andes, Apartado de Correos No. 1, Mérida 5251, Venezuela*

J. M. Besson, M. Gauthier, and A. Polian
*Physique des Milieux Condensés, Université Pierre et Marie Curie, T13-E4, 4 place Jussieu, 75252 Paris CEDEX 05, France*
(Received 9 June 1992)

The Raman-active modes of $CuGaS_2$ have been investigated at ambient temperature under high pressure using neon gas as pressure transmitting medium up to 18 GPa. An assignment of the symmetry of the zone-center modes is proposed on the basis of their pressure dependence as compared to that of the corresponding modes in zinc-blende ZnS. Under quasihydrostatic conditions and in the absence of shear stress, no broadening of lattice modes occurs prior to the transition and the metastability of the chalcopyrite lattice is shown to extend to at least 18.4 GPa, which is well into the domain of stability of the high-pressure rocksalt phase.

## I. INTRODUCTION

Semiconductors of the I-III-$VI_2$ group with the chalcopyrite structure have been actively studied in the past decades in part because of their applications in various fields of technology. They are isoelectronic analogs of the zinc-blende structure II-VI semiconductors where the replacement of the cationic sublattice by two different atomic species induces a tetragonal distortion of the cubic symmetry. Nevertheless, both for their electronic and vibrational properties, chalcopyrite-type compounds show striking analogies with their cubic homologues and this has long been successfully used to relate the properties of one family to those of the other.

The vibrational properties of the chalcopyrite family, especially the sulfides and selenides, have been investigated by the usual methods, that is, by measurements of Raman and Brillouin scattering, infrared optical properties, and, to a lesser extent, neutron scattering. Nevertheless the identification of lattice modes is sometimes incomplete,[1] even in the best studied compounds, because of the complexity of the dispersion scheme in the chalcopyrite structure. In this sense, high-pressure studies have proven to be quite powerful in resolving crowded regions of the vibrational spectrum and in helping assign the observed frequencies.

Among the I-III-$VI_2$ family the sulfides have been studied most under high pressure because their energy is in the visible range and they are thus most accessible to optical measurements. In the present work, we have studied $CuGaS_2$ up to 18 GPa by Raman scattering at ambient temperature and compared our data with previous infrared[1-4] and Raman data, at ambient,[1,5] and under high pressure.[6,7] Our conclusions lead to a reassignment of the observed frequencies, by comparison with previous[7] high-pressure work.

$CuGaS_2$, as the other chalcopyrites, undergoes a phase transition[8,9] from its low-pressure body-centered tetragonal structure (point group $I\bar{4}2m$, with two formula units per primitive cell) which has fourfold coordination of the atoms, to a high-pressure structure with sixfold coordination, which is probably rocksalt type or a slightly distorted version of it. This transition is similar in nature to the corresponding one in the IV, III-V, and II-VI families that is strongly first order with martensitic character and accompanied by a large (16%) volume decrease. The instability which propagates the transition in the binary compounds is in most observed cases linked to the edge of the zone TA($X$) phonon branch which weakens in frequency at high density. We have observed this mode up to 18.4 GPa, where its frequency had decreased to 60% of its ambient pressure value. Due to the large hysteresis of the transition, the phase line between the chalcopyrite and the NaCl structure must be placed well below this value, as well as below previously published estimates.

## II. EXPERIMENTAL PART

Single-crystal samples of undoped $CuGaS_2$ were grown by the iodine vapor transport method as described in Ref. 10. In the crystal growth experiments we produced several types of crystals which are classified by color, for convenience, as yellow, green, black, and orange. Results of their analysis by x-ray diffraction are compiled in Table I. It is clear that the green-colored crystals are closest to pure $CuGaS_2$ and therefore we used these samples for the high-pressure Raman studies. By contrast, orange-colored samples are multiphase crystals and were not used here. The typical morphology of the as-grown green single crystals is either platelet-shaped with a well-developed (112) surface or needlelike with a [111] growth axis. For the high-pressure experiments the green $CuGaS_2$ samples were prepared by lapping and polishing a piece of $p$-type plate-shaped crystal ($p=2.0\times10^{15}$ $cm^{-3}$ at 300 K) down to a thickness of 20 $\mu$m. The slabs were then cleaved into small pieces to the dimensions of the pressure chamber.

Unpolarized Raman-scattering measurements were performed in a membrane diamond-anvil cell[11] where the

 

TABLE I. Results of x-ray diffraction on several varieties of vapor grown $CuGaS_2$ (compiled from Ref. 10).

| Type | Structure | $CuGaS_2$ lattice parameters (nm) | Space group |
|---|---|---|---|
| Yellow | Cubic | $a=0.519(1)$ | $F43m$ |
| Green | Tetragonal phase | $a=0.5326(2)$ | Chalcopyrite |
| | | $c=1.0446(4)$ | $I\bar{4}2d$ |
| Black | Tetragonal $CuGaS_2$+ | $a=0.5335(2)$ | Chalcopyrite |
| | $\gamma$-CuI as impurity | $c=1.0448(4)$ | $I\bar{4}2d$ |
| Orange | Tetragonal $CuGaS_2$+ | $a=0.5326(2)$ | Additional |
| | traces of another phase: | | phase |
| | Distorted chalcopyrite | $c=1.0441(4)$ | not identified |
| | with | | distorted |
| | $a=0.5216$ nm | | chalcopyrite or |
| | $c=1.043$ nm | | superstructure |

pressure can be varied by pneumatic bellows. Neon gas was loaded under high pressure and used as a pressure-transmitting medium. The pressure was calibrated to within $\pm 0.1$ GPa by using the power five ruby luminescence scale with the pressure in GPa related to the wavelength $\lambda$ by[12]

$$P=380.8\left[\left[\frac{\lambda}{\lambda_0}\right]^5-1\right]. \quad (1)$$

The ruby samples were $\cong 4000$ ppm $Cr^{3+}$ doped and 5–15 $\mu$m in average dimensions. The spectrometer was an XY Dilor System, used in the double-monochromator OMA mode, in the backscattering geometry. The 514.5-nm ($h\nu=2.409$ eV) line of an argon laser was used at powers of 10 mW with the sample outside the cell. The laser spot was 20 $\mu$m in diameter. In the cell a power of 50 mW incident on the diamonds proved to be low enough not to cause any heating of the sample in the pressurizing medium. The resolution was better than 1 $cm^{-1}$.

## III. RESULTS

To measure the pressure coefficients of the modes, runs were done on the upstroke and downstroke up to 15 GPa only. Above this range of pressure, as will be shown later, irreversible opacity sets in, which corresponds to partial transformation to the high-pressure phase. Therefore, the data points between 15 and 18 GPa were not used to evaluate the mode Grüneisen parameters. The reason is that $CuGaS_2$ undergoes a strong first-order phase transition to a rocksalt-type structure[9] with a volume decrease of 16%. The occurrence of this transition might alter the mode frequencies of the chalcopyrite phase by size effects or inhomogeneous stress conditions and, for this part of the work the pressure was limited to under 15 GPa where the frequency variation of the modes [Figs. 1(a) and 1(b)] was reversible on the upstrokes and downstrokes.

The relative intensity and linewidths of individual modes considerably varied with pressure. This will be discussed in Sec. III B. Figures 2(a) and 2(b) show an example of this variation at two different pressures. All modes assigned here except for two of them could be observed at ambient pressure. But in the cell, the increased scattering from the diamonds and reduced volume of the sample occasionally made individual modes unobservable either because they were too weak or because they merged with a neighboring peak. On other occasions, by contrast, structures which were not observable at am-

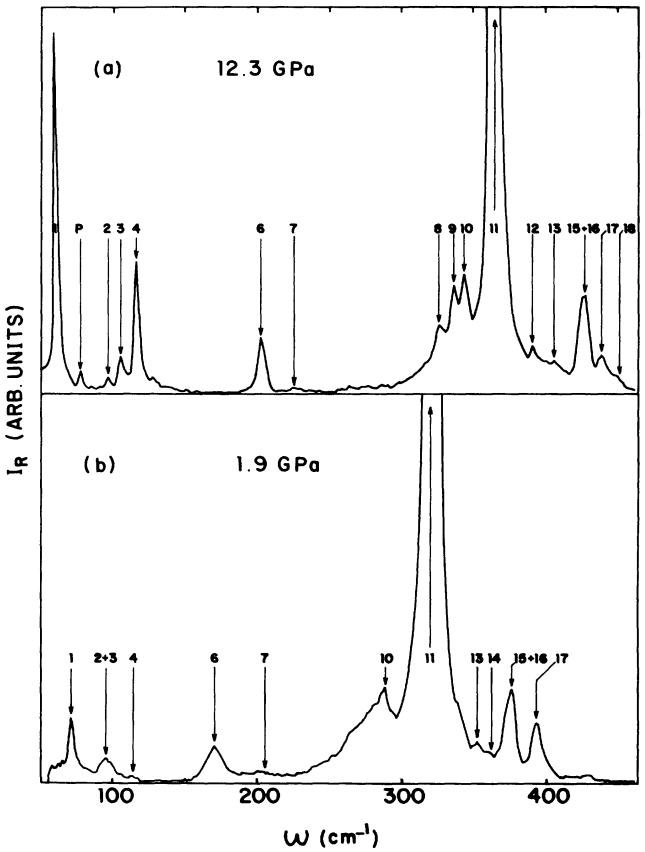


FIG. 1. $CuGaS_2$ spectra at two different pressures at 300 K. Excitation: unpolarized 514.5-nm line of argon laser in backscattering geometry, incident on (112) face of a 20-$\mu$m-thick sample. Individual modes are labeled, when identifiable, according to Table II. (a) 12.3 GPa, (b) 1.9 GPa.

bient pressure became well resolved: In Fig. 1(b), the triplet of lines 8,9,10 is clearly separated, whereas around ambient pressure, only one broad feature is observable.

For convenience we labeled the lines which are observed and discussed here from 1 to 18 and divided them into separate groups according to the zinc-blende modes they are the analogs of.

### A. Pressure dependence of the frequencies

The pressure shift of the modes is shown in Figs. 2(a) and 2(b) except for mode 5 (148 $cm^{-1}$) which could not be followed under high pressure. By contrast, frequencies 3 (99 $cm^{-1}$) and 9 (271 $cm^{-1}$) were not observable at ambient pressure but became readily visible at 3 GPa and above. Full lines in this figure are a polynomial fit of the form

$$\omega=\omega_0+aP-bP^2 \tag{2}$$

with the wave number $\omega$ in $cm^{-1}$ and $P$ in GPa.

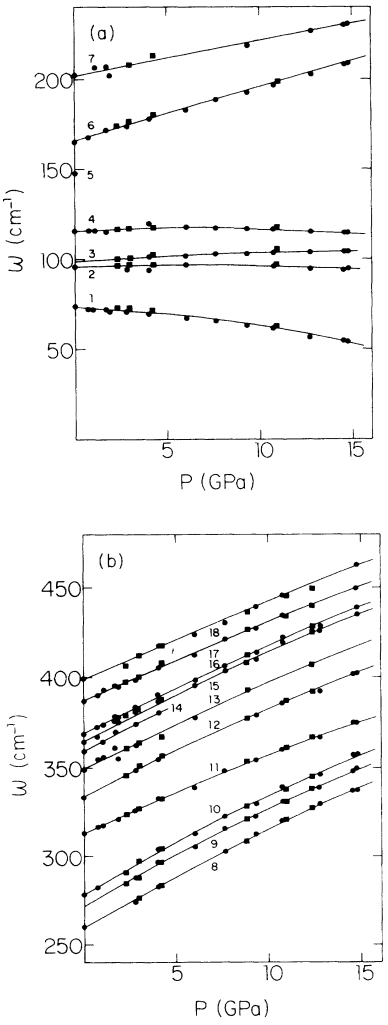


FIG. 2. Pressure dependence of Raman-active modes. ○, Upstroke. □, Downstroke. Full lines are quadratic fits [Eq. (2)] with parameters of Table II. (a) Modes 1–7, (b) modes 8–18.

The values of the parameters are listed in Table II. The choice of a second-order polynomial is not arbitrary: The bulk modulus of $CuGaS_2$ is 94 GPa (Ref. 6) and in this range of compression the relative volume variation of the crystal is less than 10%, and the pressure variation of the modes must be linear to first order with only a small second-order correction, for well-behaved modes at least, that is, those which do not go soft nor have a symmetry which may lead to a structural transition close by. There would be no justification in adding to Eq. (2) a cubic term, since even for the low-frequency modes which are involved in the phase transition as discussed later on, Eq. (2) gives a fit which is well within the experimental uncertainties.

### B. Linewidths and intensities

Two low-frequency peaks (1 and 4) have large variations of intensity with pressure, relative to their neighbors (2 and 3), and to the rest of the spectrum. To quantify this variation, one has to evaluate the Raman efficiency from the measurement of the Raman intensity. The energy gap of $CuGaS_2$ is 2.5 eV, that is, some 100 meV above the exciting light, and it separates from it at a rate[13] of 40 meV $GPa^{-1}$. To compensate for possible absorption effects at the band edge and for the variation in volume, the intensities of modes 1 and 4 was divided by the integrated intensity of mode 6 which was taken as a reference.

The Raman cross section for a Stokes process is given by

$$S\cong A|M|^2\frac{n_i+1}{\omega_i} \tag{3}$$

with $\omega_i$ the frequency of the phonon:

$$n_i=(\exp[h\omega_i/K_BT]-1)^{-1}\ . \tag{4}$$

Here the variation of the scattered light frequency is neglected and the line shape taken to be a constant. For a single two-band contribution to $M$, we have

$$M=\frac{\langle\alpha|H_a|\beta\rangle\langle\beta|H_{e\text{-ph}}|\beta\rangle\langle\beta|H_a|\alpha\rangle}{(E+\omega_i-\omega_l)(E-\omega_l)} \tag{5}$$

with $H_a$ and $H_{e\text{-ph}}$ the electron-radiation and electron-phonon interactions, $\alpha$ and $\beta$ the intermediate states separated by an energy gap $E$, $\omega_l$ the laser frequency, $\omega_i$ the frequencies of the phonons taken from the experiment.

Here, we have no evidence for the resonance of the modes with the first energy gap $E_g$ since the denominators in (5) should cause a decrease of the Raman peaks by three orders of magnitude when $E_g-h\omega_l$ increases from 100 meV at ambient pressure up to 600 meV at 15 GPa, which is not observed. We thus take any resonance to be well above 2.5 eV and have not corrected the intensities for the denominator of $M$. The observed intensities of modes 1, 4, and 5 are then corrected for the variation of the thermal population factor by means of (4) and the ratios of the reduced intensities are plotted in Fig. 3 which shows the relative increase of the Raman tensor of modes

TABLE II. Pressure dependence of Raman lines with their proposed symmetry assignment and correspondence with zinc-blende zone points.

| No. of line | $\omega_0$ ($cm^{-1}$) | $a$ ($cm^{-1}GPa^{-1}$) | $b$ ($10^2$ $cm^{-1}GPa^{-2}$) | $\frac{1}{\omega_0}\frac{d\omega}{dP}$ ($GPa^{-1}$) | Mode symmetry | Zinc-blende origin Symmetry | Group of modes | Remarks |
|---|---|---|---|---|---|---|---|---|
| 1 | 74 | −0.7 | 4.0 | 0.01 | $\Gamma_{5(L,T)}$ | $X_5$ | | Intensity increases with pressure |
| 2 | 95 | +0.3 | 2.0 | 0.003 | $\Gamma_{4(L,T)}$ | $W_2$ | TA($X_5$) | |
| 3 | 99 | 0.6 | 1.3 | 0.006 | $\Gamma_3$ | $W_2$ | | Observable only above 2 GPa |
| 4 | 116 | 0.4 | 2.7 | 0.003 | $\Gamma_{5(L,T)}$ | $W_4$ | | Intensity increases with pressure above 5 GPa |
| 5 | 148 | | | $2\times\Gamma_5$ | $X_5$ | | LA($X_3$) | Weak at ambient pressure; not observed under pressure |
| 6 | 165 | 3.0 | 0 | 0.018 | $\Gamma_{5(T,L)}$ | $W_3$ | | |
| 7 | 202 | 1.9 | 0 | 0.011 | $\Gamma_3$ | $X_3$ | | Weak; possible combination; see text |
| 8 | 258 | 6.0 | 4.0 | 0.023 | $\Gamma_{4,5(T)}$ | $W_4, W_2$ | | |
| 9 | 271 | 5.9 | 4.1 | 0.022 | $\Gamma_{5(L)}$ | $W_4$ | TO($X_5$) | Not observed below 2.5 GPa |
| 10 | 278 | 6.0 | 4.0 | 0.022 | $\Gamma_{4L}$ | $W_2$ | | |
| 11 | 312 | 4.9 | 4.4 | 0.016 | $\Gamma_1$ | $W_1$ | LO($X_1$) | |
| 12 | 332 | 5.1 | 2.0 | 0.015 | $\Gamma_{5(T)}$ | $X_5$ | | |
| 13 | 348 | 4.9 | 1.3 | 0.014 | $\Gamma_{5(L)}$ | $X_5$ | TO($X_5$) | |
| 14 | 358 | 5.0 | 0.014 | $\Gamma_3$ | $W_2$ | | | Weak at ambient pressure; not observed above 4 GPa |
| 15 | 364 | 5.0 | 3.1 | 0.014 | $\Gamma_{5(T)}$ | | Center | |
| 16 | 368 | 5.0 | 3.1 | 0.014 | $\Gamma_{4(T)}$ | $\Gamma_{15}$ | of | |
| 17 | 387 | 4.4 | 2.0 | 0.011 | $\Gamma_{5(L)}$ | | zone | Possibly double peak; see text |
| 18 | 399 | 4.4 | 1.33 | 0.011 | $\Gamma_{4(L)}$ | | $\Gamma_{15}$ | Broad shoulder |

1 and 4. Neglecting the variation of the denominator in (5) means that the increase shown in Fig. 3 is a minimum value. The actual variation may be larger.

Another peak which does not show large variations was used as a reference instead of 6: the doublet of modes 15+16, with essentially the same result for the relative variation of modes 1 and 4 within 15%.

A different type of variation occurs in the intensity of all modes when a pressure of 15 GPa is exceeded, as shown in Fig. 4 for mode 6. The decrease above this pressure is representative of the structural transition to the opaque high-pressure phase.

Linewidths of individual peaks have not been systematically studied. In Fig. 5 only three examples are given. Most modes have almost constant width with pressure such as line 1 (low frequency $\Gamma_5$) or 11 ($\Gamma_1$). The latter had been found in Ref. 7 to exhibit a remarkable increase with pressure from its original value of $\cong 5-10$ $cm^{-1}$ at 15 GPa and this had been interpreted by the authors of this reference as a sign of atomic displacement prior to the phase transition. Another explanation may be put forward: In Ref. 7 the ethanol-methanol mixture was used and the increase in width of the $\Gamma_1$ Raman peak which is reported there is that which is expected when

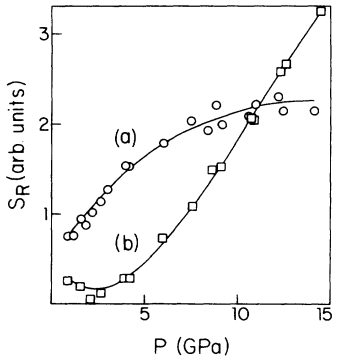


FIG. 3. Reduced intensity relative to mode 6 under pressure, of the two frequency modes: (a) mode 1, $\Gamma_5(X_5)$ (74 $cm^{-1}$ at ambient pressure); (b) mode 4, $\Gamma_5(W_4)$ (115.5 $cm^{-1}$ at ambient pressure).

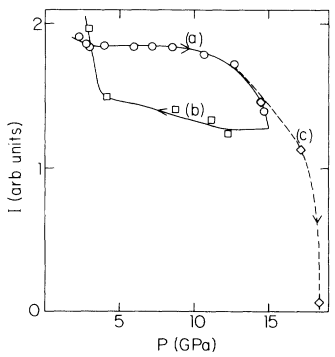


FIG. 4. Integrated intensity as a function of pressure of mode 6 (165 $cm^{-1}$ at ambient pressure); (a) upstroke to 14.5 GPa; (b) downstroke from 14.5 GPa; (c) other run: upstroke to 18.4 GPa.

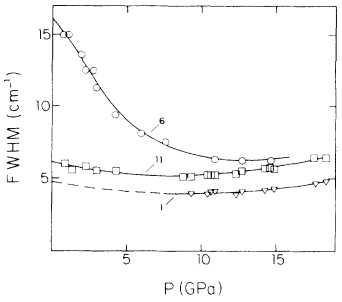


FIG. 5. Full width at half-maximum of modes; 6 [$\Gamma_5(W_3)$ (165 $cm^{-1}$)]; 11 [$\Gamma_1$ (312 $cm^{-1}$)]; 1 [$\Gamma_5(X_5)$ (74 $cm^{-1}$)].

the pressurizing medium becomes a hard glass above 10 GPa. By contrast, in our case, as shown in Fig. 5, solid neon remains plastic enough above its freezing pressure not to induce drastic pressure gradients in the sample.

This in turn allows us to take any variation in the width of individual modes as a *bona fide* effect, such as the variation in the linewidth of mode 6 which is a $\Gamma_5$ (LO-TO) doublet, the full width at half-maximum of which decreases from $\cong 16$ $cm^{-1}$ at ambient to 6 $cm^{-1}$ above 10 GPa.

## IV. ASSIGNMENT OF MODES

In discussing the high-pressure behavior and the symmetry assignment of individual modes, we shall make constant reference to the analogy of $CuGaS_2$ with its isoelectronic cubic analog ZnS, which should, as noted in the Introduction, be very similar because the masses of Ga and Cu are close to that of Zn, and the $c/a$ ratio is 1.95, which is not far from the cubic value of 2. Thus when the zone points $\Gamma$, $X$, and $W$ of zinc blende are folded into the zone center $\Gamma$ points in the chalcopyrite[14] structure, some continuity is expected in the physical properties, among which are the mode frequencies and their behavior under pressure. This approach has proven successful for the study of the electronic band structure of chalcopyrites and it will be used here for the interpretation of the vibrational modes at the center of the Brillouin zone. The body-centered tetragonal unit cell of $CuGaS_2$ contains two formula units. There is a total of 24 modes of vibration and the irreducible representation[5] at the center of the zone is

$$\Gamma = 1\Gamma_1 + 2\Gamma_2 + 3\Gamma_3 + 4\Gamma_4 + 7\Gamma_5 \ . \qquad (6)$$

Subtracting the acoustic and silent $\Gamma_2$ modes, and taking into account the LO-TO splitting in infrared-active modes leaves out 22 Raman active frequencies, out of which $2\times 9 = 18$ are infrared active.

Since the ideal chalcopyrite lattice can be interpreted as a superstructure of the zinc-blende lattice the zone-center modes can be related to the $\Gamma$, $X$, and $W$ modes of zinc blende they originate from.[1,14] Thus, in Tables II and III we have separated, for convenience, the observed modes into five groups related to five high-symmetry points in the $\Delta(\Gamma$-$X)$ direction of the zinc-blende Brillouin zone. These are the transverse-acoustic $X_5$ group with the transverse-acoustic $X_5$ point and the $W_4$ and $W_2$ points; the longitudinal-acoustic $X_3$ group with the $X_3$ point and $W_3$; the transverse-optical $X_5$ group with points $X_5$, $W_4$, and $W_2$; the $W_1$ mode coming from the $W_1$ point of the $X_1$, $W_1$ branch; the $\Gamma_{15}$ modes coming from the center of the zone mode from which the LO and TO zinc-blende phonons originate, by Coulomb splitting. This is shown on the left part of Fig. 6 where a schematic representation of the Brillouin zone of zinc blende is given, using the values of Ref. 15 for the energies of the high-symmetry points. The right part of this figure, that is, the correlation of the zinc-blende modes with the chalcopyrite ones, are discussed thereafter.

In this discussion we shall frequently refer to infrared measurements which should provide unambiguous information on the symmetry and polarization of infrared-active modes. Actually, in the case of $CuGaS_2$, contradictory reports have been made over the years.[1-4] Here we shall adopt the assignment of Ref. 1 which is a critical review of previous infrared and Raman work.

### A. Transverse-acoustic group

This is the most characteristic of the chalcopyrite structure since it reflects the behavior of the edge-of-the-zone TA modes of zinc blende when folded back onto the $\Gamma$ point. It should contain two $\Gamma_5$ modes, one $\Gamma_3$, and one $\Gamma_4$.

The assignment of mode 1 to $\Gamma_5(L,T)$ coming from the $X_3$ point is borne out by its negative pressure coefficient which is similar to that of the edge-of-the-zone acoustic phonons[16-19] in the cubic series. In other published Raman studies, only two more modes out of the remaining three had been identified in this group. Here, the use of high pressure allows us to resolve the $2+3$ doublet into two components, one of which, number 2, is infrared active. We thus assign it, in accordance with Ref. 1, to the $\Gamma_4, \Gamma_3$ doublet which originates from the $W_2$ point of zinc

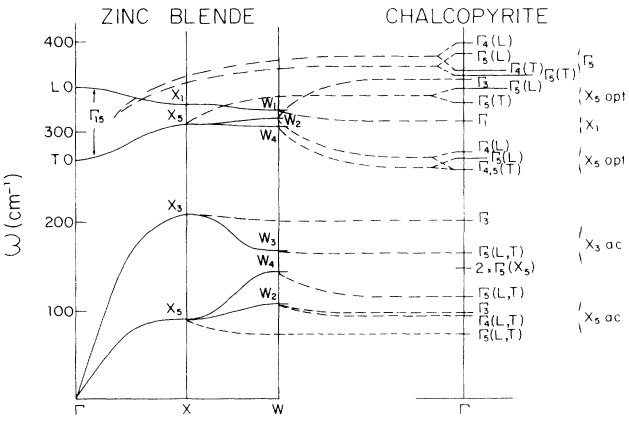


FIG. 6. Correspondence scheme of $CuGaS_2$ chalcopyrite lattice modes with ZnS blende. Energies of $\Gamma$, $X$, and $W$ zinc-blende zone points from Ref. 15. Full lines: schematic dispersion curves of zinc blende. Dashed lines connect zone-center chalcopyrite points with their correspondents in the zinc-blende zone when the latter is folded up into the chalcopyrite Brillouin zone in going from the cubic to the tetragonal lattice.

TABLE III. Comparison of our assignment with that of Refs. 1, 5, and 7.

| | This work | | | | Reference 7 | | | Reference 1 | | Reference 5 | |
|---|---|---|---|---|---|---|---|---|---|---|---|
| Zinc-blende group | No. of line | $\omega_0$ ($cm^{-1}$) | $\gamma$ | Assignment | $\omega_0$ ($cm^{-1}$) | $\gamma$ | Assignment | $\omega_0$ ($cm^{-1}$) | Assignment | $\omega_0$ ($cm^{-1}$) | Assignment |
| TA($X_5$) | 1 | 74 | −0.9 | $\Gamma_{5(L,T)}$ | 75 | −0.8 | $\Gamma_{5(L,T)}$ | 74 | $\Gamma_{5(L,T)}$ | 75.76 | $\Gamma_{5(L,T)}$ |
| | 2 | 95 | 0.3 | $\Gamma_{4(L,T)}$ | 95 | 2.0 | $\Gamma_{4(L)}$ | 95 | $\Gamma_{4(L,T)}$ | 95 | $\Gamma_{5(T)}$ |
| | 3 | 97 | 0.6 | $\Gamma_3$ | | | | 97 | $\Gamma_3$ | 98 | $\Gamma_{5(L)}$ |
| | 4 | 115.5 | 0.3 | $\Gamma_{5(L,T)}$ | 116 | 1.3 | $\Gamma_3$ | | | | |
| LA($X_3$) | 5 | 148 | | Second order | 147 | 0.8 | $\Gamma_{5(L,T)}$ | | | 147 | $\Gamma_{5(T)}$ |
| | 6 | 165 | 1.7 | $\Gamma_{5(L,T)}$ | 167 | 2.0 | $\Gamma_{5(L,T)}$ | 160/156 | $\Gamma_{5(L,T)}$ | 167 | $\Gamma_{5(L)}$ |
| | 7 | 202 | 0.9 | $\Gamma_3$ | 203 | 1.1 | Second order | 203 | $\Gamma_3$ | 203 | $\Gamma_3$ |
| | | | | Defect mode | 238 | 2.6 | $\Gamma_3$ | | | 243 | $\Gamma_3$ |
| TO($X_5$) | 8 | 258 | 2.2 | $\Gamma_{4,5(T)}$ | | | | 262 | $\Gamma_{4,5(T)}$ | 259.3 | $\Gamma_{4,5(T)}$ |
| | 9 | 271 | 2.0 | $\Gamma_{5(L)}$ | 273 | 1.4 | $\Gamma_{5(T)}$ | 276 | $\Gamma_{5(L)}$ | 278 | $\Gamma_{5(L)}$ |
| | 10 | 278 | 2.0 | $\Gamma_{4(L)}$ | 283 | 1.1 | $\Gamma_{5(L)}$ | 285 | $\Gamma_{4(L)}$ | 284 | $\Gamma_{4(L)}$ |
| | | | | | 286 | 1.1 | $\Gamma_{4(T)}$ | | | | |
| | | | | | 288 | 1.7 | $\Gamma_{4(L)}$ | | | | |
| LO($X_1$) | 11 | 312 | 1.8 | $\Gamma_1$ | 312 | 1.5 | $\Gamma_1$ | 312 | $\Gamma_1$ | 312 | $\Gamma_1$ |
| TO($X_5$) | 12 | 332 | 1.4 | $\Gamma_{5(T)}$ | 332 | 1.4 | $\Gamma_{5(T)}$ | 335 | $\Gamma_{5(T)}$ | 335 | $\Gamma_{5(T)}$ |
| | 13 | 348 | 1.3 | $\Gamma_{5(L)}$ | 347 | 1.5 | $\Gamma_{5(L)}$ | 352 | $\Gamma_{5(L)}$ | 352 | $\Gamma_{5(L)}$ |
| | 14 | 358 | 1.3 | $\Gamma_3$ | | | | 358 | $\Gamma_3$ | | |
| Zone | 15 | 364 | 1.3 | $\Gamma_{5(T)}$ | 367 | 1.5 | $\Gamma_{5(T)}$ | 363 | $\Gamma_{5(T)}$ | 365 | $\Gamma_{5(T)}$ |
| center | 16 | 368 | 1.3 | $\Gamma_{4(T)}$ | 367 | 1.5 | $\Gamma_{4(T)}$ | 368 | $\Gamma_{4(T)}$ | 371 | $\Gamma_{4(T)}$ |
| $\Gamma_{15}$ | 17 | 387 | 1.1 | $\Gamma_{5(L)}$ | 385 | 1.3 | $\Gamma_{5(L)}$ | 384 | $\Gamma_{5(L)}$ | 387 | $\Gamma_{5(L)}$ |
| | | | | | 393 | 1.4 | $\Gamma_{4(L)}$ | | | | |
| | 18 | 399 | 1.0 | $\Gamma_{4(L)}$ | 401 | | $\Gamma_3$ | 401 | $\Gamma_{4(L)}$ | 401 | $\Gamma_{4(L)}$ |

blende and is weakly split by the tetragonal distortion.

The remaining $\Gamma_5$ mode is then assigned to line 4. This is justified by the behavior of this line under high pressure (Fig. 3). It increases in intensity under pressure as does mode 1 and it is thus logical to assign it the same symmetry.

### B. The LA ($X$) group

In this region two modes are expected: one infrared-active $\Gamma_5$ mode and the $\Gamma_3$ which originates from the zinc-blende $X_3$ point. The latter can readily be assigned to mode 6 which is a weakly split (4 $cm^{-1}$) LO, TO doublet, as shown by infrared measurements.[3]

A problem then arises in assigning the remaining $\Gamma_3$ mode to either lines 5 and 7, or to another frequency which has been observed by only two authors at 238 $cm^{-1}$ in Ref. 7 and 243 $cm^{-1}$ in 5. In other studies, including the present one, this mode has not been observed. This may lie in the nature of the crystals used which in those two references are of the "orange" variety whereas other authors studied green-colored samples. As mentioned in Sec. II orange-colored crystals are known to be multiphase systems and we propose that the extra line observed by the authors of Refs. 5 and 7 is to be assigned to this type of defect.

Line 5 was observed at room pressure in the present work but in contrast to Ref. 7 was too weak to be followed under high pressure presumably because of different selection rules due to a different orientation of the crystal axes in the cell. We will therefore use here the pressure dependence observed in Ref. 7 for the discussion. This mode has a very small variation under pressure, and decreases by a few $cm^{-1}$ in 15 GPa. This is exactly what would be expected from a combination mode of the edge-of-the-zone TA branch of the chalcopyrite structure, which all but joins, at the zone edge, with the lowest optical branch, that is, the 74-$cm^{-1}$ line. This branch must be quite flat since the TA branch frequency of zinc-blende structure of II-VI semiconductors in the $X$ direction is almost wave-vector independent over half of the zone.[20,21] The pressure dependence of the combination mode should thus be that of the zinc-blende TA phonons at the midpoint of the zone edge and the $\Gamma$ point. This is shown to be zero or slightly negative,[21] in complete accordance with the observed behavior. Thus we assign the 148-$cm^{-1}$ line to a $2\times74$ $cm^{-1}$ combination.

The only remaining peak, number 7, then has to be assigned to the $\Gamma_3$ mode, in accordance with most other authors, as shown in Tables II and III.

To conclude this subsection, a *caveat* is in order: Although line 7 has almost always been assigned to $\Gamma_3$, it has also been proposed to be a combination line of the (97,95 $cm^{-1}$) doublet. Indeed it is a broad and weak feature which is found[22] to almost disappear at 13 K which would support the latter assignment.

### C. The transverse-optical group

In chalcopyrite crystals, the modes in this group which originate from the $X_5$ (TO) branch of zinc blende ($1\times\Gamma_4$, $1\times\Gamma_3$, and $2\times\Gamma_5$) are split into two sections by the strong $\Gamma_1$ mode which originates from the $W_1$ ($X_1$) point.

The low-frequency section contains three lines which, on the basis of infrared data[1,3,4] can unambiguously be assigned to a $\Gamma_4$ and a $\Gamma_5$ mode. Here, by contrast with Ref. 1, we place the origin of the $\Gamma_5$ mode at the $W_4$ point of the zinc-blende zone and not at the $X_5$ point because the pressure dependence of this triplet of lines is quite different from that of the $X_5$ point as discussed in Sec. V. Apart from this, our assignment fits (Table II) with other authors with the exception of Ref. 7 where two extra lines are reported which have not been reported in any other work. Examination of the experimental evidence presented in Fig. 1 by the authors of Ref. 7 does not support the existence of four separate modes in this region.

The high-frequency part of this group (lines 12,13) can then be readily assigned from infrared data. Line 14 thus has to be a $\Gamma_3$ mode which originates from the $W_2$ point. The large splitting between the $\Gamma_4$ and $\Gamma_3$ modes which originates from the $W_2$ point seems a bit surprising in view of the small separation of the low-frequency $\Gamma_3$-$\Gamma_4$ doublet. Nevertheless this seems to be a constant feature of the sulfur chalcopyrites series[1] where the $\Gamma_3$ ($W_2$opt) mode has consistently been found to lie in between the $X_5$opt group and the $\Gamma_{15}$ one, not only in $CuGaS_2$, but also in $AgGaS_2$ and $CuAlS_2$. This is also borne out by calculations which consistently[1] place this mode above the $\Gamma_1$ frequency.

### D. The $\Gamma_{15}$ group

The remaining four frequencies (15,16,17,18) can be assigned to the $\Gamma_5$ and $\Gamma_4$ modes which originate from the $\Gamma_{15}$ point of the zinc-blende zone center. Here again, infrared data should give an unambiguous assignment.

Nevertheless, a problem remains for line 18 which is assigned to $\Gamma_4(L)$. This shows up in Raman data as a weak and broad shoulder on the side of line 17. At low temperature[22] (13 K) the latter splits into an ill-resolved doublet of two frequencies some 7 $cm^{-1}$ apart and line 18 has all but disappeared. Even at ambient temperature, mode 17 can be deconvoluted into two frequencies at 384 and 388 $cm^{-1}$. If the latter were to be assigned to $\Gamma_4(L)$ the weak feature of 400 $cm^{-1}$ would have to be a combination mode.

### E. Summary

This assignment is compared with that of other authors in Table III, with the exception of Ref. 6 where only a limited number of lines were observed, 12 in all, out of which 7 were followed under pressure. This was undoubtedly due to the opacity of the highly iron-doped sample that was used there. In any case the assignment of the modes essentially fits with Ref. 1 and the Grüneisen parameters of all modes but one are the same as in Ref. 7.

The attribution of modes that we propose is in excellent agreement with Ref. 1. The agreement is good with Ref. 5 for the modes which originate from the optical modes of zinc blende but unsatisfactory for the acoustical group of frequencies. By contrast the assignment of Ref. 7 is clearly at variance with ours, as well as with the other two references examined.

A potential explanation for those discrepancies must lie in the quality of the samples, since samples used in all studies, including ours, must have contained defects, as shown by their color. These defects may be Raman active, as indicated by the discrepancies in the observed frequencies.

## V. DISCUSSION

### A. Pressure coefficients of the modes

In the course of the assignment procedure, reference has been made to the pressure coefficients of the modes. Those which originate from the $X$ and $\Gamma$ points of the zinc-blende structure, the pressure coefficients of which are known from experiment and/or calculations can well be identified in this way as shown in Table IV. In this table, we have compared the variation in frequency of the modes between ambient pressure and 15 GPa with the dispersion curves at ambient pressure and 15 GPa for ZnS, given in Ref. 18. The latter are based on ambient pressure neutron data and a calculation of the dispersion curves at 15 GPa that fits with the experimental values for the edge-of-the-zone frequencies which have been measured under pressure.

The similarity of the pressure variation of $CuGaS_2$

TABLE IV. Variation of the frequencies of $CuGaS_2$ modes between ambient pressure and 15 GPa, compared to that of corresponding ZnS modes in the same pressure interval, as reported in Ref. 17.

| ZnS | | | $CuGaS_2$ | |
|---|---|---|---|---|
| Mode symmetry | $\Delta\omega/\omega$ (%) | No. of line | Mode symmetry | $\Delta\omega/\omega$ (%) |
| $TA(X_5)$ | −29 | 1 | $\Gamma_5(X_5)$ | −26 |
| $LA(X_3)$ | 17 | 7 | $\Gamma_3(X_3)$ | 15 |
| $TO(X_5)$ | 19 | 12,13 | $\Gamma_{5(L,T)}(X_5)$ | 18 |
| $LO(X_1)$ | 19 | 11 | $\Gamma_1(W_1)$ | 17 |
| | | 16 | $\Gamma_{4,5(T)}$ | 20 |
| $TO(\Gamma_{15})$ | 21 | 17 | $\Gamma_{5(L)}$ | 17 |
| $LO(\Gamma_{15})$ | 15 | 18 | $\Gamma_{4(L)}$ | 16 |

modes with their ZnS ($X$) or ($\Gamma$) analogs is evident. In this table we also included a mode ($\Gamma_1$) originating from $W$ since the $\Gamma_1 \rightarrow W_1$ dispersion curve should be quite flat[15] and should experience little deformation under pressure.

This procedure nevertheless cannot be used for $W$ points in general, especially when they split into two components. It may be noted that the $\Gamma_4$-$\Gamma_5$ ($W_2$) triplet of lines has a common Grüneisen constant of $\cong 2$ which separates it from the other frequencies and points to its having a common origin $W_2$ but *not* $X_5$. Indeed the pressure variation of these lines (8, 9, and 10) between ambient pressure and 15 GPa amounts to 29% which is quite different from the increase in frequency of the $X_5$ point which is only 19%.

This type of comparison of pressure coefficients is rather straightforward for ZnS-type chalcopyrites where the different groups of modes are well separated in frequency. By contrast it may prove to be a decisive criterion in other chalcopyrites, such as the selenides, to identify the modes originating from the $X_3$ acoustical branch which get mixed up with those coming from the $X_5$ optical branch because of the small energetic distance between the LA and the TO branches at the edge-of-the-zone in ZnSe for instance.

### B. Intensity and linewidth variation

The decrease in the linewidth of mode 6 ($\Gamma_{5L,T}$) which we noted in the previous section is noticeable enough to deserve some comment. Since this line corresponds to a TO,LO doublet, it would be tempting to assign this decrease in linewidth to a decrease of the LO-TO distance coming from the expected decrease of the ionic charge under pressure. This cannot be retained because we would then expect a slow continuous decrease with pressure, and also expect to observe this decrease of the Coulomb splitting on other LO-TO modes, neither of which is observed. This decrease in linewidth then has to be ascribed to the separation, under pressure, of the $\Gamma_5$ mode from another mode with which it overlaps at ambient pressure. This must be a two-phonon density of states from the lower bands since the silent $\Gamma_2$ modes are predicted to be higher in energy.

The increase in intensity of the lowest-frequency $\Gamma_5$ modes (74 and 115 $cm^{-1}$) cannot be entirely ascribed to variations in the thermal occupation number, or in the frequency of the modes, as shown in Fig. 3. Therefore, it points to an increase of the electron-phonon interaction presumably as the transition pressure is approached. An analogous effect has been observed on the $2\times$TA modes of zinc-blende ZnSe (Ref. 16) which increase in intensity by an order of magnitude between 5 and 12 GPa where the phase transition occurs, this increase being larger than would be expected from the pressure evolution of a two-phonon combination with constant Raman tensor.

It is tempting in both cases to invoke an increase of the electron-phonon interaction, as the low-frequency shear mode decreases. In this structural class, the phase transition on the upstroke commonly occurs when the frequency of the edge-of-the-zone TA phonon, in zinc blende, or its counterpart in $CuGaS_2$, has decreased[7] by about 30%. This corresponds to halving ($0.7^2 = 0.5$) the spring constant of the corresponding harmonic oscillator and must come from a noticeable redistribution under pressure of the density of electrons which are responsible for the restoring force of this bond. When this shear bond becomes weaker under high pressure, the corresponding electronic levels should be more perturbed by the displacements of the atoms under the eigenvectors of the phonon, which in turn will lead to an increase of the electron-phonon interaction and of the Raman tensor.

This can be put forward only as a proposal, since under the conditions of the present experiment the pressure variation of the intensity of $\Gamma_5$ modes is far from accurate and might also be assigned, for instance, to antiresonance effects, or variations in the symmetry-forbidden part of the Raman intensity which may evolve as the tetragonal distortion varies under pressure. Experiments using a better defined geometry and several exciting laser lines would provide a more exact measure of this effect, which, if confirmed, certainly would give insight into the mechanism of this type of phase transition in zinc-blende and chalcopyrite structures.

## VI. PHASE TRANSITION

Although the analysis of the phase transition process in $CuGaS_2$ is not the main part of this work, the observation of the Raman intensity gives useful information in this transformation. The integrated intensity of the 165-$cm^{-1}$ $\Gamma_5(W_3)$ which we took as a reference was shown in Fig. 4. At 15 GPa on the upstroke, the decrease in intensity of the signal corresponds to the initiation of the transition when precipitates of the high-pressure phase and/or slip planes and structural defects[23] occur, which diffuse and absorb the incident and scattered light. Even at 18.4 GPa, the phase transition is not complete and despite the decrease in intensity of the signal by a factor of 25 with respect to ambient pressure, a perfectly good Raman signal of the chalcopyrite phase can be obtained with the mode frequencies located close to their expected values from the parameters in Table II. The transition pressure has been reported to be some 16 GPa in Refs. 7 and 9. This is not a contradiction: In the above references, the ethanol-methanol mixture was used, which is known to induce severe stress inhomogeneity above 10 GPa. This is favorable to initiate the actual transformation earlier than in our case where solid neon was used. The pressure is much more homogeneous than in ethanol-methanol (cf. Fig. 5 and Ref. 7) but since there are fewer low-symmetry nucleation centers, induced by shear, the low-pressure phase is metastably preserved further up into the stability domain of the high-pressure variety. Thus it cannot be stated that either 16 or 18.5 GPa is a "better" value for the thermodynamic transition line between the chalcopyrite and the rocksalt structures of $CuGaS_2$. Both values are underestimates. Indeed, curve (b) in Fig. 4 shows that, on the downstroke, the crystal starts resuming its transparency around 5 GPa. This is indicative of reversal to the low-pressure fourfold-coordinated structure, which may be chalcopy-

rite or disordered zinc blende.[13] Both structures can be taken as equivalent for this discussion since they must have very similar free energies. Taking the midpoint between the initiation of the direct and reverse transitions, one would evaluate the transition line to lie in the vicinity of 10 GPa, as a rough estimate. This is not unexpected and it has been shown[23] that in this type of transformation from fourfold- to sixfold-coordinated structures, hysteresis of several GPa may well occur.

This evaluation of the stability domain of $CuGaS_2$ is given here only as an indication and must be confirmed by further experimental work. Nevertheless, the observation of the characteristic Raman spectrum of $CuGaS_2$ as high as 18.4 GPa when stress distributions are homogeneous deserves some comment. The fact that the observed Raman intensity was reduced to 29% of the original value by absorption from the opaque high-pressure phase does *not* mean that most of the crystal had already transformed. If, for argument's sake, we take the rocksalt-type crystallites to be metallic or semimetallic with an absorption coefficient of $\alpha \cong 10^4\ \mathrm{cm}^{-1}$ as an order of magnitude, it can be easily calculated that only 10% of the sample volume need be transformed and homogeneously dispersed in the crystal to decrease the Raman signal from the remaining 90% chalcopyrite to 29% of its original value. Full transformation under the conditions of this experiment will lie at a somewhat higher pressure.

This observation in turn raises a few questions on the relation between the frequency variation of the low-frequency shear mode (TA in zinc blende, $\Gamma_5$ in chalcopyrites) and the initiation of the phase transition. A useful phenomenological relation[7] has been put forward for this type of structure noting that the phase transition occurs when the shear mode has decreased by $(30\pm5)\%$ from its ambient pressure value, that is, for a decrease of $\cong 50\%$ of the relevant spring constant. Here the spring constant of $CuGaS_2$ has decreased by 65% to one-third of its original value at 18.4 GPa, when the transition is far from completed. By contrast, at the pressure instability of the chalcopyrite structure, on the upstroke, which should be under 13 GPa, the decrease of the force constant is less than 35%, whereas at $\cong 16.5$ GPa, where the transition is observed in the ethanol-methanol mixture, the decrease in the spring constant is 50%. There is, therefore, quite a difference between the electronic configuration which exists at the pressure where chalcopyrite becomes thermodynamically unstable (10–12 GPa?) and that which exists at the actual phase transition [16 to over 20 GPa (Ref. 9), depending on the experimental conditions]. Since only the former can be predicted by theory, it is not surprising that, in the few cases where the instability due to shear modes was calculated[24] in the phase transition of zinc-blende structures, the transition pressure was predicted to be much lower than actually observed. To avoid this difficulty there is no choice but to perform measurements at high temperature to reduce the hysteresis and the metastability problems to extrapolate an accurate high-temperature phase diagram down to low temperature.

## VII. CONCLUSION

The following conclusions can sum up the results of this work.

(1) The behavior of lattice modes of $CuGaS_2$ under high pressure has been utilized to identify the symmetry of Raman-active modes.

(2) Center-of-the-zone modes of this chalcopyrite have pressure coefficients which are remarkably similar to those of the corresponding zinc-blende zone points.

(3) The center-of-the-zone $\Gamma_5$ mode which corresponds to the edge-of-the-zone TA vibration has been observed to weaken in frequency down to 59% of its ambient pressure value, and possibly to increase in intensity because of increasing electron-phonon interaction.

(4) The decrease in frequency of this mode is a consequence of the weakening of the noncentral bond which ultimately also causes the instability of the chalcopyrite lattice but it does not drive the transition and, in the absence of shear, the metastability of the lattice can be maintained well into the stability domain of the high-pressure phase.

(5) The use of neon as a pressure transmitting medium allows precise observation of the line shapes, in contrast to ethanol-methanol which causes severe pressure gradients. In particular, contrary to previous statements, the $\Gamma_1$ mode in $CuGaS_2$ does not broaden under pressure and its pressure dependence remains regular up to 18.4 GPa which is well within the domain of instability of the chalcopyrite phase. Its regular decrease in intensity can be ascribed to decreasing resonance with the band-gap state with increasing pressure.

(6) Determination of the elastic constant tensor of chalcopyrite under pressure by Brillouin scattering would be quite desirable to understand the mechanism of the high-pressure phase transition. Inelastic neutron scattering data up to $\cong 15$ GPa also would be useful to measure the evolution of dispersion curves. Finally, the transition in $CuGaS_2$ is probably more complex than a two-phase transformation, with at least disordered zinc blende as an intermediate modification on the downstroke. The precise mechanism of this transformation could be derived from either imaging plate x-ray powder diffraction, or elastic neutron diffraction under high pressure.

## ACKNOWLEDGMENTS

Part of this work was performed within the framework of a CNRS and CEFI-PCP Materials (France) and CONICIT (Venezuela) international collaboration program. J.G. and B.J.F. are grateful to the Consejo de Desarrollo Cientifico y Tecnologico (CDCHT) of the Universidad de Los Andes for financial support. One of us (B.J.F.) wishes to thank J. C. Chervin for assistance during his visit at the Physique des Milieux Condensés Laboratory. Physique des Milieux Condensés is Unité Associé No. URA 0782 of the CNRS.

[1]W. H. Koschel and M. Bettini, Phys. Status Solidi B **72**, 729 (1975).
[2]J. Baars and W. H. Koschel, Solid State Commun. **11**, 1513 (1972).
[3]W. H. Koschel, F. Sorger, and J. Baars, J. Phys. **36-C3**, 177 (1975).
[4]S. Sugai, J. Phys. Soc. Jpn. **43**, 5992 (1977).
[5]J. P. van der Ziel, A. E. Meixner, H. M. Kasper, and J. Ditzenberger, Phys. Rev. B **9**, 4286 (1974).
[6]M. Bettini and W. B. Holzapfel, Solid State Commun. **16**, 27 (1975).
[7]C. Carlone, D. Olego, A. Jayaraman, and M. Cardona, Phys. Rev. B **22**, 3877 (1980).
[8]A. Jayaraman, V. Narayanamurti, H. M. Kasper, M. A. Chin, and R. G. Maines, Phys. Rev. B **14**, 3516 (1976).
[9]A. Werner, H. D. Hocheimer, and A. Jayaraman, Phys. Rev. B **23**, 3836 (1981).
[10]M. Delgado (unpublished).
[11]R. Le Toullec, J. P. Pinceaux, and P. Loubeyre, High Press. Res. **1**, 77 (1988).
[12]H. K. Mao, P. M. Bell, J. W. Shaner, and D. J. Steinberg, J. Appl. Phys. **49**, 3276 (1978).
[13]J. González and C. Rincón, J. Phys. Chem. Solids **51**, 1093 (1990).
[14]G. D. Holah, J. S. Webb, and H. Montgomery, J. Phys. C **7**, 3875 (1974).
[15]D. N. Talnar and B. K. Agrawal, Phys. Status Solidi B **64**, 71 (1974).
[16]G. Weill, J. C. Chervin, and J. M. Besson, High Press. Res. **7**, 105 (1991).
[17]B. A. Weinstein and G. J. Piermarini, Phys. Rev. B **12**, 1172 (1975).
[18]B. A. Weinstein, Solid State Commun. **24**, 595 (1977); B. A. Weinstein, in *High Pressure Science and Technology,* edited by K. D. Timmerhous and M. S. Barber (Plenum, New York, 1979), Vol. 1, p. 141.
[19]R. Trommer, H. Mueller, M. Cardona, and P. Vogl, Phys. Rev. B **21**, 4869 (1980).
[20]N. Vagelatos, D. Wehe, and J. S. King, J. Chem. Phys. **60**, 3613 (1974).
[21]B. Hennion, F. Morissa, G. Pepy, and K. Kunc, Phys. Lett. **36A**, 376 (1971).
[22]J. González, J. Guinet, and H. Fontaine (unpublished).
[23]J. M. Besson, J. P. Itié, A. Polian, G. Weill, J. L. Mansot, and J. González, Phys. Rev. B **44**, 4214 (1991).
[24]K. Kunc and R. M. Martin, Phys. Rev. B **24**, 2811 (1981).